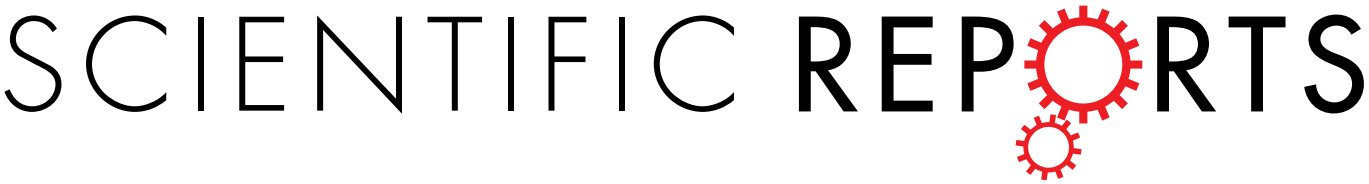

OPEN

Gate dependence of upper critical field in superconducting (110) $LaAlO_3/SrTiO_3$ interface

Received: 16 January 2016
Accepted: 03 June 2016
Published: 05 July 2016

S. C. Shen[1], B. B. Chen[2], H. X. Xue[1], G. Cao[2], C. J. Li[1], X. X. Wang[1], Y. P. Hong[1], G. P. Guo[2], R. F. Dou[1], C. M. Xiong[1], L. He[1] & J. C. Nie[1]

The fundamental parameters of the superconducting state such as coherence length and pairing strength are essential for understanding the nature of superconductivity. These parameters can be estimated by measuring critical parameters such as upper critical field, H_{c2}. In this work, H_{c2} of a superconducting (110) $LaAlO_3/SrTiO_3$ interface is determined through magnetoresistive measurements as a function of the gate voltage, V_G. When V_G increases, the critical temperature has a dome-like shape, while H_{c2} monotonically decreases. This relationship of independence between the variation of T_c and of H_{c2} suggests that the Cooper pairing potential is stronger in the underdoped region and the coherence length increases with the increase of V_G. The result is as for high temperature superconducting cuprates and it is different than for conventional low temperature superconductors.

Oxide heterostructures have attracted much attention in recent years due to a plethora of novel or enhanced physical phenomena observed at interfaces[1,2]. For example, the *two dimensional electron gas* (2DEG) formed at the interface between two perovskite insulators, $LaAlO_3$ (LAO) and $SrTiO_3$ (STO), becomes superconducting[3] at around 200 mK. This discovery triggered intense investigations of the superconductivity mechanism[4–8] at interfaces. A number of intriguing properties emerge at the superconducting interface. Literature indicate on a pseudogap-like behavior[9], on the electron pre-formed pairing[10], and on the coexistence of superconductivity and ferromagnetism[11–13]. The phase diagram for an interface is similar to that of high temperature superconducting (HTS) cuprates[7,9]. The interface exhibits superconductivity for an extremely low carrier density[14,15]. Presented aspects may indicate on unconventional pairing mechanism. Nevertheless, the conventional electron-phonon coupling has been also considered[5,16]. Therefore, the microscopic mechanism responsible for interface superconductivity is still unclear and more research is of high interest.

Recently, it was reported that an energy gap persists above the superconducting dome defined as the variation of the critical temperature, T_c, vs. carrier doping. Furthermore, the energy gap increases monotonically as the gate voltage V_G decreases. This correlation indicates on a pseudogap-like behavior of (001) LAO/STO interfaces[9] and it is opposite to the V_G dependence of the superfluid density[14]. For additional information about electron pairing in interfaces, it is useful to determine fundamental superconducting parameters such as the coherence length, ξ_0, and the strength of pairing potential. These parameters can be extracted from upper critical field, H_{c2}; a higher H_{c2} means a smaller coherence length and a stronger pairing potential[17]. Previous investigations of H_{c2} have shown that superconductivity observed for (001) or (110) LAO/STO interfaces is of two dimensional nature[3,18–20], but the V_G dependence of H_{c2} that is associated to pairing strength while being distinct from the superfluid density, has not been reported. Noteworthy is also that most studies are focused on (001) LAO/STO, while the (110) system is less explored although its study can bring an important contribution to understanding of superconductivity at interfaces[20–22].

In this work we report the dependence of H_{c2} on V_G in a superconducting 2DEG (110) LAO/STO interface. We found that H_{c2} decreases when V_G increases. At the same time, the $T_c(V_G)$ curve shows a dome-like shape (with a maximum). Our results indicate that the Cooper pairing potential becomes stronger in the underdoped regime.

Results and Discussions

Critical temperature, critical current and normal state resistance as a function of gate voltage.

In Fig. 1 are presented as examples, curves of (interface or sheet) resistance, R_s, versus temperature for three

[1]Department of Physics, Beijing Normal University, Beijing 100875, China. [2]Key Laboratory of Quantum Information, CAS, University of Science and Technology of China, Hefei, Anhui 230026, China. Correspondence and requests for materials should be addressed to G.P.G. (email: gpguo@ustc.edu.cn) or J.C.N. (email: jcnie@bnu.edu.cn)

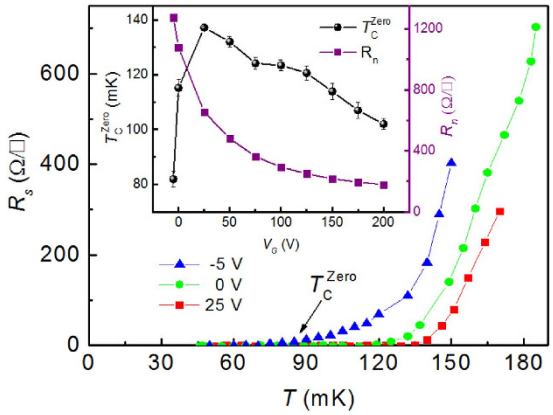

Figure 1. The resistance R_s of the (110) LAO/STO interface as a function of temperature at three representative gate voltages and for $B = 0$ T. The inset shows the gate voltage V_G dependence of the critical temperature T_C^{Zero} and of the normal state resistance R_n. The maximum of the T_C^{Zero} (V_G) curve is at 138 mK and at 25 V. Lines are guide to the eyes.

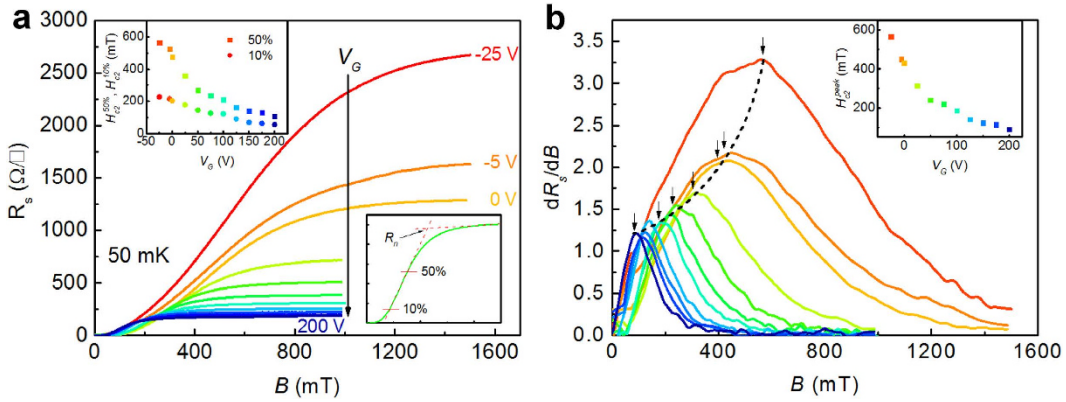

Figure 2. (**a**) Curves of $R_s(B)$ for $-5 \leq V_G \leq 200$ V at 50 mK. The inset in the right corner shows determination of R_n, $H_{c2}^{50\%}$ and $H_{c2}^{10\%}$. The inset in the left corner shows $H_{c2}^{50\%}(V_G)$ and $H_{c2}^{10\%}(V_G)$ curves at 50 mK; (**b**) Curves of dR_s/dB vs. B at 50 mK. Arrows indicate points of maximum of these curves and dashed line is guide for eyes. Magnetic field of a maximum point is defined as H_{c2}^{peak}. The inset shows variation of H_{c2}^{peak} as a function of V_G.

different gate voltages (−5 V, 0 V and 25 V) under zero magnetic field. Temperature for which R_s drops below the detection limit of the measuring equipment defines the critical temperature, T_C^{Zero} (Fig. 1). The curve of T_C^{Zero} as a function of V_G (in zero magnetic field) has a dome-like shape with a maximum at 25 V (Fig. 1 inset). The dome-like shape of the T_C^{Zero} (V_G) curves was previously observed in LAO/STO and (001) $LaTiO_3/SrTiO_3$ (LTO/STO) interfaces[7,20,23]. A dome-like shape with a maximum at $V_G = 25$ V is also obtained for the variation of the critical current $I_c(V_G)$. The critical current, I_c, was determined at 50 mK from I-V curves measurements (see Supplementary Information, Fig. S1). The $T_C^{Zero}(V_G)$ and $I_c(V_G)$ similar dome-like dependencies indicate a strong influence of the carrier density on T_C^{Zero} and I_c.

From the measurements of R_s with magnetic field (up to 1.6 T) applied perpendicular to the surface of the interface at a fixed temperature and gate voltage one can determine the normal state resistance, R_n. An example of $R_s(B)$ curves at 50 mK and for V_G from −25 to +200 V is presented in Fig. 2a. Inset to Fig. 2a shows for selected (T, V_G) values how R_n is determined. Namely, R_n is the resistance of the cross point between the fitting lines of the steepest part of the $R_s(B)$ experimental curve and of the region where R_s almost saturates. For a fixed temperature (50 mK), one $R_n(V_G)$ curve is plotted in Fig. 1 inset. Enhancement of V_G decreases R_n. Curve is non-linear and the decrease rate is smaller for higher V_G.

It is remarkable that V_G can tune superconducting and normal state characteristics such as T_C^{Zero} and R_n, respectively. Results suggest that V_G influences 2DEG superconductivity features and the carrier density. Our results are consistent with literature[20].

Upper critical field as a function of gate voltage. For a fixed temperature and V_G, the upper critical field H_{c2} is determined as the field where resistance is 10%, 50% of R_n in the $R_s(B)$ curves (Fig. 2a inset, right corner). This methodology was used to determine H_{c2} for different superconducting systems[24–26]. We note that magnetic field B is applied in this work only perpendicular to the interface surface. Reported articles[19,20] indicate that

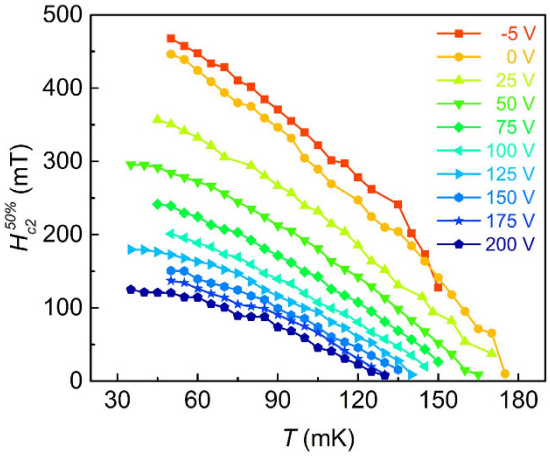

Figure 3. Temperature dependence of $H_{c2}^{50\%}$ for different V_G. Lines are guide for the eyes.

H_{c2} shows large anisotropy when B is applied in-plane and out-of-plane. At 50 mK, the $H_{c2}^{10\%}(V_G)$ or $H_{c2}^{50\%}(V_G)$ (Fig. 2 inset, left corner) curves are unexpectedly without a dome-like shape that is specific for the $T_C^{Zero}(V_G)$ and $I_c(V_G)$ (Figs 1 and S1) curves. Namely, for a lower V_G, H_{c2} monotonically increases (Fig. 2 inset, left corner). At the same time, a decrease of V_G below $V_{G,\,max} = 25$ V counter-intuitively produces the decrease of both T_C^{Zero} and I_c (Figs 1 and S1).

The differential curves dR_s/dB as a function of B, obtained from $R_s(B)$ data (Fig. 2a) for different V_G and at 50 mK, are presented in Fig. 2b. Each curve displays a peak (marked with an arrow in Fig. 2b). The peak shifts to higher B and its intensity increases when V_G decreases. The magnetic field of the peak, denoted H_{c2}^{peak}, as a function of V_G (at 50 mK) is shown in Fig. 2b, inset. A dome-like shape is not obtained and, as expected, this curve has a similar behavior as $H_{c2}^{10\%}(V_G)$ or $H_{c2}^{50\%}$. (V_G) curves. Furthermore, the values of H_{c2}^{peak} and of $H_{c2}^{50\%}$ are close to each other, but we shall keep both parameters in the discussion because of their different background: $H_{c2}{}^{50\%}$ is arbitrary taken, while $H_{c2}{}^{peak}$ defines the inflexion point of the $R_s(B)$ cur. The inflexion point may have a physical meaning and, hence, $H_{c2}{}^{peak}$ can be more sensitive to external factors than $H_{c2}^{50\%}$.

Figure 3 shows curves of $H_{c2}^{50\%}(T)$ for different V_G from −5 V up to 200 V. For all gate voltages, $H_{c2}^{50\%}$ increases with temperature decrease. Curves of $H_{c2}^{50\%}$. (T) shift into the region of higher values of $H_{c2}^{50\%}$-T for decreasing V_G. This enhancement occurs even for negative V_G, where a lower V_G induces a lower T_C^{Zero}. Moreover, the slope $(dH_{c2}^{50\%}/dT|_{Tc})$ of the $H_{c2}^{50\%}(T)$ curve approaching $H_{c2}^{50\%}(T_c) = 0$ systematically increases when V_G decreases. The overall observed tendency does not change, if we use in the analysis $H_{c2}^{10\%}$ or H_{c2}^{peak} instead of $H_{c2}^{50\%}$ (Fig. S2 a,b). According to Ginzburg-Landau (GL) theory, near T_c the upper critical field is a linear function of $(T_c - T)$ and smoothly saturates when lowering the temperature. Our results suggest an anomalous unconventional behavior of the upper critical field vs. temperature, and it is no longer appropriate to describe this dependence using the GL theory. The $H_{c2}^{10\%,\,50\%,\,peak}(T = 0\,K)$ values obtained by linear extrapolation of e data at low temperature are increasing with decreasing V_G. The determination of H_{c2} at $T = 0$ K lacks precision. However, if we estimate the relative H_{c2}-increase (δH_{c2}) at a finite temperature (e.g. 60 mK) between the curves for $V_G = -5$ V and $V_G = 0$ V, a criterion closer to $R_s = 0$ shows a lower value (i.e. $\delta H_{c2}^{10\%} = 1.3\%$, while $\delta H_{c2}^{50\%} = 5.5\%$). This finds its understanding in the following: The emergence of $R_s = 0$ is due to the global superconductivity. With increasing magnetic field, a finite resistance occurs, and, hence, global superconductivity disappears. However, local superconductivity still exists before the system recovers to normal state. Thus, it is reasonable that we observe a larger H_{c2} for a more negative V_G. This indicates that Cooper pair can persist up to a higher magnetic field than the upper critical field corresponding to global superconductivity.

Superconductor-insulator transition. The magnetic-field-induced superconductor-insulator transition(SIT)[27] shows a characteristic fan-shaped pattern of $R_s(B)$ isotherms crossing at one point. For example, in Fig. 4a the SIT cross point for $V_G = -5$ V is at 810 mT. The $R_s(T)$ curves extracted from $R_s(B)$ show a plateau for 810 mT (Fig. 4b). The plateau separates two regimes. Therefore, the magnetic field drives a continuous quantum phase transition from a superconducting 2DEG to a weakly insulating state. Further finite-size scaling analysis shows that the data can be collapsed onto a bi-value curve (Fig. 4a, inset). It results that the crossing point is a *q*uantum *c*ritical *p*oint (QCP), at which the phase transition occurs. Literature often show magnetic-field-induced SIT for different 2D superconductors[27,28], including for interfaces such as LAO/STO and (001) LTO/STO[29,30].

As already noted, $H_{c2}(T)$ for a fixed V_G depends on the criterion adopted for the H_{c2} determination in the case of a broad transition[26,31] and the $H_{c2}(T = 0\,K)$ cannot be determined in a reliable manner. This situation questions the intrinsic nature of the H_{c2} – enhancement (for a lower V_G) in the underdoped region. Due to this, here we use another method to directly determine the zero - temperature upper critical field, $H_{c2}^{*}(T = 0\,K)$. This method is independent of the criterion applied to $R_s(B)$ curves. At the QCP, taken as a transition point between superconducting and normal states of the 2DEG, the corresponding magnetic field is defined as $H_{c2}^{*}(T = 0\,K)$. The

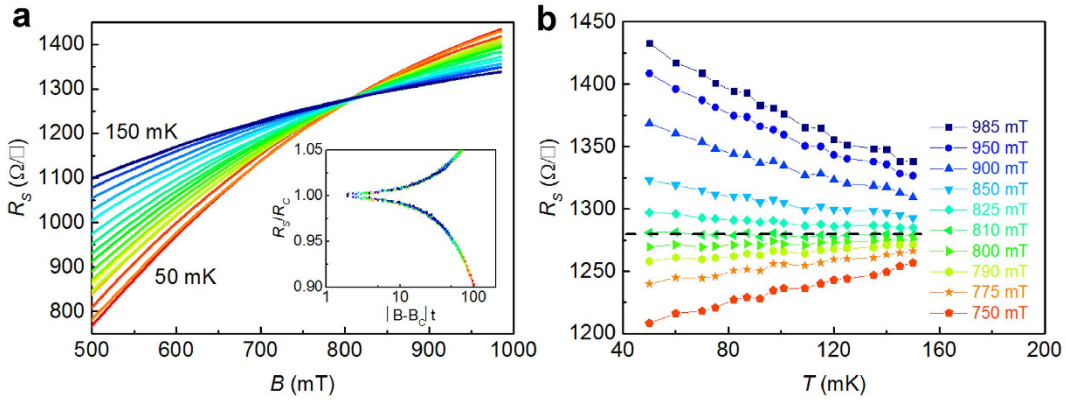

Figure 4. (**a**) SIM pattern: curves of $R_s(B)$ at different temperatures for $V = -5$ V. Note the crossing point at 810 mT that defines the *q*uantum *c*ritical *p*oint (QCP) with ($B_c = 810$ mT, $R_c = 1297.54\,\Omega$). The inset shows the bi-value curve obtained by collapse of the date by finite-size scaling analysis. (**b**) Curves of $R_s(T)$ at different magnetic fields B and for $V_G = -5$ V. Dashed line shows a plateau corresponding to QCP. Continuous lines are guide for the eyes.

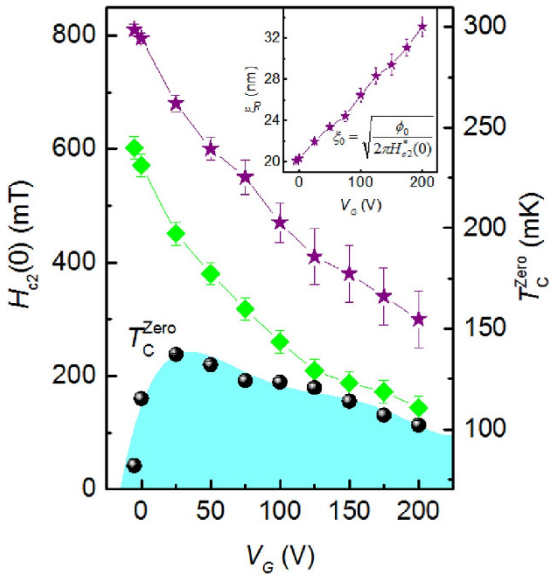

Figure 5. The V_G dependence of T_C^{Zero}, $H_{c2}^{50\%}$ (T = 0 K) (green diamonds) and H^*_{c2} (T = 0 K). (violet stars). The inset shows the V_G dependence of the coherence length $\xi_0 = \sqrt{\Phi_0/2\pi H^*_{c2}}$ where Φ_0 is the quantum flux. Continuous lines are guide for the eyes.

H^*_{c2}(T = 0 K) curve as a function of V_G is plotted in Fig. 5. Although it is considered that this method does not give accurate values of H^*_{c2}(T = 0 K)[30], this barely affects our main results, the dependence on V_G of H^*_{c2}(T = 0 K) being similar to that of $H_{c2}^{50\%}(T = 0\,\text{K})$ (Fig. 5). One reason for a non-precise determination of H^*_{c2}(T = 0 K) vs. V_G is: when $V_G \neq -5$ V, e.g., a $V_G = 75$ V is used for the construction of the magnetic-field-induced SIT pattern, the crossing point of the $R_s(B)$ isotherms transforms into a field domain centered at 0.55 T and extending over ± 0.05 T (Fig. S3a). In this case, the conventional power-law scaling behavior fails to describe the quantum criticality (Fig. S3b). Multiple quantum criticality was also found and reported for the (001) LTO/STO interface[29]. The phenomenon of multiple critical exponents suggests an unconventional critical behavior of SIT in the (110) LAO/STO interface, and it will be discussed elsewhere.

Phase diagram. The superconducting phase diagram of the (110) LAO/STO interface is presented in Fig. 5. As already addressed in the previous sections, the upper critical field H_{c2} independently of the criterion for its determination monotonically increases when V_G decreases, while T_C^{Zero} displays a dome-like curve with a maximum. In the inset to Fig. 5 is shown the GL coherence length ξ_0 determined from H_{c2} as a function of V_G. The most striking anomalous result is enhancement of H_{c2} accompanied by the decrease of ξ_0 for decreasing V_G, i.e. for the carrier depletion reflected by the dome-like curve in the underdoped region. Results indicate that the Cooper pairing potential is stronger in the underdoped region.

A systematic increase in H_{c2} with decreasing doping has been reported both in high-T_c cuprates and iron-based superconductors[31,32]. This is usually considered as an evidence for the existence of a so-called 'pseudogap' state, in which the bosonic pairs form above T_c but cannot condensate into superconducting state due to dilution of pairs[33]. Recently, the planar tunneling spectroscopy study in 2DEG at a (001) LAO/STO interface has shown that the energy gap Δ increases with charge carrier depletion in both underdoped and overdoped regions[9]. And, the coherence-peak-broadening parameter Γ derived from the Dynes fit, that is related to the strength of the superconducting pairing interaction, increases steeply with decreasing V_G. GuangLei Cheng *et al.*[10] recently reported that the Cooper pairs form at temperatures well above the superconducting transition temperature of the (001)LAO/STO superconducting system. In the experiments they used a superconducting single-electron transistor and they observed that pairs condensate at low magnetic fields and temperatures. The physical understanding of the processes at (110) LAO/STO interface is analogous to that of hole-doped cuprates[31], namely, the pairing potential is stronger and the Ginzburg-Landau coherence length ξ_0 decreases in the underdoped region as V_G decreases. The trend differs from that of superfluid density and superconducting transition temperature[7,14]. Namely, the superfluid density decreases with decreasing V_G providing that the phase fluctuation is important[14,34,35]. The observation of Δ/Γ scaled with T_c in ref. 9 implies that the limited quasiparticle lifetime controls T_c effectively[9], and the reduction in T_c versus Δ was attributed to a competing order parameter or to a weak phase coherence. In addition, in LAO/STO system the spin-orbit coupling is non negligible and strongly depends on V_G[36,37]. Both conventional and unconventional pairing mechanisms have been considered to describe superconductivity in interfaces[5,6,16,38]. For example, the spin-orbit coupling[36,37] and the coexistence of superconductivity and ferromagnetism[11–13] may indicate formation of possible exotic superconducting states such as finite momentum Cooper pairing[39,40]. One has also to consider a different orbital reconstruction between (001) and (110) systems[20,41]. Superconducting properties and Rashba spin-orbit coupling can be largely tuned by controlling selective orbital occupancy in different crystal orientations[20]. For the underdoped region, it has been reported that a Lishiftz transition is observed at (001) interface[42,43]. The (110) system is expected to be characterized only by a $3d_{xz}/d_{yz}$ filled electronic state; thus the superconducting properties of the (110) interface system can be substantially different from that of the (001) system.

Conclusions

We systematically investigated the upper critical field as a function of gate voltage by ultralow temperature magnetoresistance measurements in superconducting 2DEG of a (110) LAO/STO interface. We found that upper critical field increases as the gate voltage decreases. Two independent methods to determine the upper critical field give a similar trend. This implies that the pairing potential is stronger in the underdoped region. This observation is similar to recent reports that consider a pseudogap-like behavior at the (001) LAO/STO interface. Our results for an interface with a different orientation contribute to understanding of the pairing mechanism of superconductivity at LAO/STO interface.

Method

A five-unit-cell $LaAlO_3$ thin film was grown on the (110) $SrTiO_3$ substrate (500 μm thickness) by pulsed laser deposition. Details were described in ref. 19. A metallic back gate was evaporated and attached to the rear of the substrate. Leakage current was low (below the maximum value of 5 nA at $V_G = 200$ V). Standard four-terminal resistance measurements were made using wedge-bonding contacts. The sample was cooled in a dilution refrigerator with a base temperature of 10 mK. The measurement current is sufficiently low (~50 nA) to avoid sample heating at ultralow temperatures. To ensure the reversible behavior of the superconductivity, the gate voltage was ramped up to 200 V after cooling down. Perpendicular magnetic field B was applied to the sample (interface) surface and the field direction is the same for all measurements.

References

1. Hwang, H. Y. Atomic control of the electronic structure at complex oxide heterointerfaces. *MRS bulletin* **31,** 28–35 (2006).
2. Hwang, H. Y. *et al.* Emergent phenomena at oxide interfaces. *Nat. Mater.* **11,** 103–113 (2012).
3. Reyren, N. *et al.* Superconducting interfaces between insulating oxides. *Science* **317,** 1196–1199 (2007).
4. Michaeli, K., Potter, A. C. & Lee, P. A. Superconducting and ferromagnetic phases in $SrTiO_3/LaAlO_3$ oxide interface structures: possibility of finite momentum pairing. *Phys. Rev. Lett.* **108,** 117003 (2012).
5. Boschker, H., Richter, C., Fillis-Tsirakis, E., Schneider, C. W. & Mannhart, J. Electron-phonon Coupling and the Superconducting Phase Diagram of the $LaAlO_3/SrTiO_3$ Interface. *Sci. Rep.* **5,** 12309 (2015).
6. Scheurer, M. S. & Schmalian, J. Topological superconductivity and unconventional pairing in oxide interfaces. *Nat. Commun.* **6,** 6005 (2015).
7. Caviglia, A. D. *et al.* Electric field control of the $LaAlO_3/SrTiO_3$ interface ground state. *Nature* **456,** 624–627 (2008).
8. Gariglio, S., Gabay, M., Mannhart, J. & Triscone, J.-M. Interface superconductivity. *Physica C: Superconductivity and its Applications* **514,** 189–198 (2015).
9. Richter, C. *et al.* Interface superconductor with gap behaviour like a high-temperature superconductor. *Nature* **502,** 528–531 (2013).
10. Cheng, G. L. *et al.* Electron pairing without superconductivity. *Nature* **521,** 196–199 (2015).
11. Dikin, D. *et al.* Coexistence of superconductivity and ferromagnetism in two dimensions. *Phys. Rev. Lett.* **107,** 056802 (2011).
12. Bert, J. A. *et al.* Direct imaging of the coexistence of ferromagnetism and superconductivity at the $LaAlO_3/SrTiO_3$ interface. *Nat. Phys.* **7,** 767–771 (2011).
13. Li, L., Richter, C., Mannhart, J. & Ashoori, R. C. Coexistence of magnetic order and two-dimensional superconductivity at $LaAlO_3/SrTiO_3$ interfaces. *Nat. Phys.* **7,** 762–766 (2011).
14. Bert, J. A. *et al.* Gate-tuned superfluid density at the superconducting $LaAlO_3/SrTiO_3$ interface. *Phys. Rev. B* **86,** 060503 (2012).
15. Lin, X., Zhu, Z., Fauqué, B. & Behnia, K. Fermi Surface of the Most Dilute Superconductor. *Phys. Rev. X* **3,** 021002 (2013).
16. Klimin, S., Tempere, J., Devreese, J. & Van Der Marel, D. Interface superconductivity in $LaAlO_3/SrTiO_3$ heterostructures. *Phys. Rev. B* **89,** 184514 (2014).
17. Tinkham, M. *Introduction to superconductivity*. (Courier Corporation, 2012).
18. Reyren, N. *et al.* Anisotropy of the superconducting transport properties of the $LaAlO_3/SrTiO_3$ interface. *Appl. Phys. Lett.* **94,** 112506 (2009).

19. Han, Y. L. *et al.* Two-dimensional superconductivity at (110) $LaAlO_3/SrTiO_3$ interfaces. *Appl. Phys. Lett.* **105,** 192603 (2014).
20. Herranz, G. *et al.* Engineering two-dimensional superconductivity and Rashba spin-orbit coupling in $LaAlO_3/SrTiO_3$ quantum wells by selective orbital occupancy. *Nat. Commun.* **6,** 6028 (2015).
21. Herranz, G., Sanchez, F., Dix, N., Scigaj, M. & Fontcuberta, J. High mobility conduction at (110) and (111) $LaAlO_3/SrTiO_3$ interfaces. *Sci. Rep.* **2,** 758 (2012).
22. Annadi, A. *et al.* Anisotropic two-dimensional electron gas at the $LaAlO_3/SrTiO_3$ (110) interface. *Nat. Commun.* **4,** 1838 (2013).
23. Biscaras, J. *et al.* Two-dimensional superconducting phase in $LaTiO_3/SrTiO_3$ heterostructures induced by high-mobility carrier doping. *Phys. Rev. Lett.* **108,** 247004 (2012).
24. Fournier, P. & Greene, R. Doping dependence of the upper critical field of electron-doped $Pr_{2-x}Ce_xCuO_4$ thin films. *Phys. Rev. B* **68,** 094507 (2003).
25. Fuchs, G. *et al.* High-Field Pauli-Limiting Behavior and Strongly Enhanced Upper Critical Magnetic Fields near the Transition Temperature of an Arsenic-Deficient $LaO_{0.9}F_{0.1}FeAs_{1-\delta}$ Superconductor. *Phys. Rev. Lett.* **101,** 237003 (2008).
26. Vedeneev, S., Piot, B., Maude, D. & Sadakov, A. Temperature dependence of the upper critical field of FeSe single crystals. *Phys. Rev. B* **87,** 134512 (2013).
27. Goldman, A. Superconductor-insulator transitions. *Int. J. Mod. Phys. B* **24,** 4081–4101 (2010).
28. Gantmakher, V. F. & Dolgopolov, V. T. Superconductor-insulator quantum phase transition. *Physics-Uspekhi* **53,** 1–49 (2010).
29. Biscaras, J. *et al.* Multiple quantum criticality in a two-dimensional superconductor. *Nat. Mater.* **12,** 542–548 (2013).
30. Mehta, M. *et al.* Magnetic field tuned superconductor-to-insulator transition at the $LaAlO_3/SrTiO_3$ interface. *Phys. Rev. B* **90,** 100506 (2014).
31. Wang, Y. *et al.* Dependence of upper critical field and pairing strength on doping in cuprates. *Science* **299,** 86–89 (2003).
32. Kohama, Y. *et al.* Doping dependence of the upper critical field and Hall resistivity of $LaFeAsO_{1-x}F_x$($x = 0$, 0.025, 0.05, 0.07, 0.11, and 0.14). *Phys. Rev. B* **79,** 144527 (2009).
33. Timusk, T. & Statt, B. The pseudogap in high-temperature superconductors: an experimental survey. *Rep. Prog. Phys.* **62,** 61 (1999).
34. Uemura, Y. *et al.* Universal Correlations between T_c and n_s/m^*(Carrier Density over Effective Mass) in High-T c Cuprate Superconductors. *Phys. Rev. Lett.* **62,** 2317 (1989).
35. Emery, V. & Kivelson, S. Importance of phase fluctuations in superconductors with small superfluid density. *Nature* **374,** 434–437 (1995).
36. Shalom, M. B., Sachs, M., Rakhmilevitch, D., Palevski, A. & Dagan, Y. Tuning spin-orbit coupling and superconductivity at the $SrTiO_3/LaAlO_3$ interface: a magnetotransport study. *Phys. Rev. Lett.* **104,** 126802 (2010).
37. Caviglia, A. *et al.* Tunable Rashba spin-orbit interaction at oxide interfaces. *Phys. Rev. Lett.* **104,** 126803 (2010).
38. Stephanos, C., Kopp, T., Mannhart, J. & Hirschfeld, P. Interface-induced d-wave pairing. *Phys. Rev. B* **84,** 100510 (2011).
39. Michaeli, K., Potter, A. C. & Lee, P. A. Superconducting and ferromagnetic phases in $SrTiO_3/LaAlO_3$ oxide interface structures: possibility of finite momentum pairing. *Phys. Rev. Lett.* **108,** 117003 (2012).
40. Loder, F., Kampf, A. P. & Kopp, T. Superconductivity with Rashba spin–orbit coupling and magnetic field. *Journal of Physics: Condensed Matter* **25,** 362201 (2013).
41. Pesquera, D. *et al.* Two-Dimensional electron gases at $LaAlO_3/SrTiO_3$ interfaces: orbital symmetry and hierarchy engineered by crystal orientation. *Phys. Rev. Lett.* **113,** 156802 (2014).
42. Joshua, A., Pecker, S., Ruhman, J., Altman, E. & Ilani, S. A universal critical density underlying the physics of electrons at the $LaAlO_3/SrTiO_3$ interface. *Nat. Commun.* **3,** 1129 (2012).
43. Stornaiuolo, D. *et al.* Tunable spin polarization and superconductivity in engineered oxide interfaces. *Nat. Mater.* **15,** 278–283 (2016).

Acknowledgements

Authors gratefully acknowledge the technical assistance of Haiou Li with transport measurements. We also would like to thank Badica Petre for useful discussions. This work was supported by the Ministry of Science and Technology of China (Grants Nos 2013CB921701, 2013CBA01603, and 2014CB920903) and the National Natural Science Foundation of China (Grants Nos 11474022, 51172029, 11374035, and11422430).

Author Contributions

J.C.N., G.P.G. and S.C.S. proposed and designed experiments. S.C.S., C.J.L. and Y.P.H. prepared the samples. S.C.S. performed the measurements with the assistance from B.B.C. and G.C. Results were analyzed by J.C.N., S.C.S., H.X.X. and X.X.W. The manuscript was written by S.C.S. and J.C.N. and discussed with C.M.X., R.F.D. and L.H. All authors discussed and contributed with comments regarding results and the manuscript.

Additional Information

Supplementary information accompanies this paper at http://www.nature.com/srep

Competing financial interests: The authors declare no competing financial interests.

How to cite this article: Shen, S. C. *et al.* Gate dependence of upper critical field in superconducting (110) $LaAlO_3/SrTiO_3$ interface. *Sci. Rep.* **6**, 28379; doi: 10.1038/srep28379 (2016).